Statistical discrimination of global post-seismic ionosphere effects under geomagnetic quiet and storm conditions

Tamara Gulyaeva & Feza Arikan

Published online: 25 Oct 2016.

Submit your article to this journal ⌇

Article views: 586

View related articles ⌇

View Crossmark data ⌇

Citing articles: 5 View citing articles ⌇

Taylor & Francis
Taylor & Francis Group

Statistical discrimination of global post-seismic ionosphere effects under geomagnetic quiet and storm conditions

Tamara Gulyaeva 🆔[a] and Feza Arikan 🆔[b]

[a]IZMIRAN, Moscow, Russia; [b]Department of EEE, Hacettepe University, Ankara, Turkey

ABSTRACT

The retrospective statistical analysis of total electron content (TEC) is carried out using global ionospheric maps (GIM) for 1999–2015. TEC anomalies are analysed for 2670 earthquakes (EQ) from M6.0 to M10.0 classified into 2205 'non-storm' EQs and 465 'storm' EQs during geomagnetic storms. The geomagnetic storms are specified by relevant thresholds of geomagnetic indices AE, aa, ap, $ap(\tau)$ and Dst. Using sliding-window statistical analysis, moving daily–hourly TEC median μ for 15 preceding days with estimated variance bounds is obtained for each grid pixel of GIM-TEC maps. The derived ionosphere variability index, $V\sigma$, is expressed in terms of ΔTEC deviation from the median normalized by the standard deviation σ. $V\sigma$ index segmentation is introduced specifying TEC anomaly if an instant TEC is outside the bound of $\mu \pm 1\sigma$. Efficiency of EQ impact on the ionosphere ($E\sigma$) is growing with EQ magnitude and depth representing relative density of TEC anomalies within area of 1000 km radius around EQ hypocentre. Positive TEC 'storm' anomalies are twice as much as those of non-storm values. This observation supports dominant post-EQ TEC enhancement with $E\sigma$ peak decreasing during 12 h for daytime but growing by nighttime during 6 h after EQ followed by gradual recovery afterwards.

1. Introduction

The effects of earthquakes in the ionosphere are subject of intense studies during recent decades (Davies & Baker 1965; Koshevaya et al. 1997; Liu et al. 2006a, Liu et al. 2006a, 2006b; Astafyeva & Heki 2009; Astafyeva et al. 2009; Harrison et al. 2010; Hayakawa & Hobara 2010; Lin 2010; Arikan et al. 2012; Lin 2012; Astafyeva et al. 2013; Komjathy et al. 2013; Pohunkov et al. 2013; Devi et al. 2014; Perevalova et al. 2014). The diversity of pre-earthquake phenomena, such as local magnetic field variations, electromagnetic emissions at the different frequency ranges, excess radon emanation from the ground, changes in water chemistry, water condensation in the atmosphere leading to haze, fog or clouds, and atmospheric gravity waves rising up to the ionosphere, induces changes in the ionospheric total electron content (TEC) and the F2 layer peak electron density (Pulinets et al. 2003; Chen et al. 2004; Pulinets & Boyarchuk 2004; Rishbeth 2006; Liu et al. 2006a, 2006b; Depueva et al. 2007; Varotsos et al., 2008, 2011; Karatay et al. 2010; Le et al. 2011; Namgaladze et al. 2012; Freund 2013; Devi et al. 2014; Akhoondzadeh 2015; Heki & Enomoto 2015). Changes in magnetic field at the time of the earthquakes have been observed and reported in various publications such as Johnston et al. (1981), Yen et al. (2004) and Varotsos et al. (2009). Modification of the electric field and currents due to electric processes in the lithosphere and the lower atmosphere (Varotsos &

CONTACT   Feza Arikan   ✉ arikan@hacettepe.edu.tr

Alexopoulos 1984a; Varotsos & Alexopoulos 1984b) is supposed to induce the co-seismic disturbances in the ionosphere (Kuo et al. 2011; Pulinets & Davidenko 2014). Dependence of larger ionospheric TEC precursors (within 1 h before EQ) on larger earthquake magnitudes is reported by Heki and Enomoto (2015). According to the acoustic mechanism, the internal atmospheric gravity waves are generated both before and after the earthquakes (Hegai et al. 2006; Koshevaya et al. 2012). The speed of the earthquake-induced acoustic gravitational wave propagation through the ionosphere can reach 990 m/s as detected with GPS network up to the sound speed at ionospheric heights, and these effects in the ionosphere are observed at distances up to 2000 km from the hypocentre (Astafyeva et al. 2009). These waves propagate in the atmosphere where their amplitudes increase relative to height due to the decrease in air density. The disturbed conditions in the ionosphere cause electromagnetic waves in the VLF band (Davies & Baker 1965; Ralchovski & Christolov 1985; Hayakawa & Hobara 2010; Athanasiou et al. 2011). In a review of expected electromagnetic and magnetic precursors, Uyeda et al. (2009) have highlighted that adequate focus needs to be given to the study of non-seismological short-term precursors, in addition to up-gradation of seismological networks.

Typically, geomagnetic storms affect large portions of globe after the anomalous changes in IMF-B, global electric currents and have patterns that can be recognized in the geomagnetic field. The pre-earthquake disturbances in the ionosphere can be observed locally or regionally depending on the type, magnitude and depth of the earthquake as indicated in various studies including Arikan et al. (2012). Though it is difficult to distinguish between pure seismic precursors in the ionosphere from geomagnetic storms effects (Afraimovich & Astafyeva 2008; Karatay et al. 2010; Devi et al. 2014), the post-earthquake phenomena are well observed and found over the local areas of high seismic activity providing opportunity to investigate both temporal and spatial earthquake–ionosphere associations (Artu et al. 2001; Athanasiou et al. 2011; Astafyeva et al. 2013; Pohunkov et al. 2013; Devi et al. 2014; Perevalova et al. 2014).

The earthquake related changes in surrounding geomagnetic field have been detected experimentally in Liu et al. (2006b) and Xu et al. (2013). Signatures of seismic-ionospheric precursors have been analysed with electron density (Ne) and electron temperature (Te) measured onboard DEMETER satellite at 630 km altitude with a spatial distribution from few degrees to almost 20° equatorward from the hypocentre (Athanasiou et al. 2011; Liu et al. 2014). The prolonged impact and frequency of the earthquakes occurrence may have cumulative effects on the ionosphere structure and variability (Astafyeva et al. 2009; Gulyaeva et al. 2014).

Liu et al. (2006a) investigated the relationship between variations in the plasma frequency at the ionospheric F2 peak, foF2, and 184 earthquakes with magnitude $M > 5.0$ during 1994–1999 in the Taiwan area excluding geomagnetic storm related events. The pre-earthquake ionospheric anomalies, defined as an abnormal decrease more than about 25% of the ionospheric foF2 during the afternoon period, between 1200 and 1800 LT, occurred within five days before the earthquakes. An advantage of investigation of the earthquake-related ionospheric phenomena in the region surrounding the hypocentre has been also confirmed by different authors (Depueva et al. 2007; Astafyeva et al. 2009; Harrison et al. 2010; Athanasiou et al. 2011; Le et al. 2011; Komjathy et al. 2013; Pohunkov et al. 2013; Liu et al. 2014).

Statistical analysis of seismic activity during 1964–2013 reveals that 13% of earthquakes $M5.0+$ from the total database of more than 79,000 EQs occurred during 1305 geomagnetic Dst storms for the same period (Gulyaeva 2014). In the present study, we focus on the ionosphere post-seismic effects for earthquakes of magnitude $M6.0$ to $M10.0$ ($M6.0+$) at the regions surrounding the hypocentre within the radius of 1000 km under geomagnetic quiet and storm conditions. The relevant cells of IONEX global map (Mannucci et al. 1998; Hernandez-Pajares et al. 2009) in the vicinity of EQ hypocentre are selected according to the size of the surrounding spatial region (Marekova 2014).

The statistical analysis applied to TEC data is described in Section 2. The criteria for classification of the data set into geomagnetic storm and non-storm conditions and the global distribution of the relevant EQs $M6.0+$ occurrence are provided in Section 3. The period of study ranges from January,

1999, to December, 2015, according to the availability of GIM-TEC maps and results of analysis are provided in Section 4. The goal of this study is to obtain new evidence on seismic-ionospheric associations which are summarized in the Conclusions in Section 5.

2. The statistical analysis of TEC data

In this study, statistical data analysis is performed using global ionospheric maps (GIM) of the TEC provided by Jet Propulsion Laboratory (JPL). TEC is defined as the line integral of plasma density in the Earth's atmosphere and it provides an estimate of the total number of free electrons inside a cylinder with 1 m^2 cross-section area in the column from the bottom of the ionosphere (65 km) to the GPS orbit of 20,200 km. The TEC is an important observable in analysis of temporal variability of the ionosphere and the plasmasphere both under quiet and under storm conditions.

The GIM-TEC maps are generated in a continuous operational way by several Data Analysis Centers since 1998, covering the period more than the entire solar cycle (Hernandez-Pajares et al. 2009). The vertical TEC is modelled by JPL in a solar-geomagnetic reference frame using bi-cubic splines on a spherical grid; a Kalman filter is used to solve simultaneously for instrumental biases and vertical TEC on the grid as stochastic parameters (Manucci et al. 1998). GIM-TEC have been initially provided with 2 h time resolution which are linearly interpolated in time to 1 h resolution, and the hourly files are provided by JPL since December 2008. The JPL maps are generated in the denser map grids ($-90{:}2{:}90°$ in latitude, $-180{:}2{:}180°$ in longitude), and time specified for 0.5:1.0:23.5 h UT so these maps are preprocessed by linear interpolation into standard IONEX format for 0:1:23 h UT. The IONEX global map consists of 5183 grid values binned in 87.5° S to 87.5° N in step of 2.5° in latitude, 180° W to 180° E in step of 5° in longitude. The similar structure of map grids is applied when the source GIM-TEC maps are converted to geomagnetic coordinates binned in $-87.5°$ N to 87.5° N in steps of 2.5° in geomagnetic latitudes, and 0° E to 360° E in steps of 5° in geomagnetic longitude using the International Geomagnetic Reference Field (IGRF) model.

According to Liu et al. (2006a), the recurrence time of the $M \geq 5.0$ earthquakes is 14.2 days. Therefore, in order to determine the reference background TEC distribution, we compute the sliding median of every successive 15 days of TEC at each grid point of the map. In the present study, we use TEC sliding median defined by a 15-day moving window, and the median value is assigned to the final day of the window, i.e. to the 15th day of the window. We use such type of 'forward' median approach because it has a potential for development of forecasting model similar to those in Gulyaeva et al. (2013); Muchtarov et al. (2013):

$$\mu_{m;d_s - d_i}(l) = \text{median}(x_{d_i}(l)...x_{d_s}(l)). \tag{1}$$

In the above equation, x denotes the GIM-TEC value at grid point l. d_i and d_s represent the first day and the final day of the sliding window, respectively. The subscript m indicates the map under investigation. Statistical study of an ionospheric parameter includes determination of median and dispersion, i.e. variability of the parameter around its median. The standard deviation σ represents a measure of the dispersion of distribution which can be computed as

$$\sigma(l) = \sqrt{\frac{1}{N_T} \sum_{1}^{N_T} (x_d(l) - \mu_{m;d_s-d_l}(l))}, \tag{2}$$

where N_T denotes total number of days in the sliding window which is set to 15 in this case. An interval within one standard deviation around the median accounts for approximately 68% of the dataset, while two and three standard deviations account 95% and 99.7%, respectively.

Table 1. Magnitude of the ionosphere variability, $V\sigma$, determined as TEC deviation from 15-day sliding median of hourly TEC (ΔTEC), normalized by the estimated variance bound, σ.

$V\sigma$	ΔTEC	Ionosphere state
4	$+3\sigma \leq \Delta\text{TEC}$	Extreme positive $V\sigma p$ anomaly
3	$+2\sigma \leq \Delta\text{TEC} < +3\sigma$	Intense positive $V\sigma p$ anomaly
2	$+1\sigma \leq \Delta\text{TEC} < +2\sigma$	Moderate positive $V\sigma p$ anomaly
1	$0 < \Delta\text{TEC} < +1\sigma$	Quiet $V\sigma p$ state
0	$\Delta\text{TEC} = 0$	Reference Quiet state
−1	$-1\sigma < \Delta\text{TEC} < 0$	Quiet $V\sigma n$ state
−2	$-2\sigma < \Delta\text{TEC} \leq -1\sigma$	Moderate negative $V\sigma n$ anomaly
−3	$-3\sigma < \Delta\text{TEC} \leq -2\sigma$	Intense negative $V\sigma n$ anomaly
−4	$\Delta\text{TEC} \leq -3\sigma$	Extreme negative $V\sigma n$ anomaly

The measure of TEC variability is further investigated as the TEC deviation (ΔTEC) from the median μ, normalized by the standard deviation σ for N_t number of days prior to and during day d_s:

$$D\sigma_d(l) = \frac{x_d(l) - \mu_{m;d_s-d_l}(l)}{\sigma(l)}. \tag{3}$$

The algorithm is completed by introducing $D\sigma$ segmentation with thresholds shown in Table 1 to result in the ionosphere variability $V\sigma$ index with magnitudes from $V\sigma n = -4$ (extreme negative TEC anomaly) in step of $\Delta V\sigma = 1$ to $V\sigma p = +4$ (extreme positive TEC anomaly). $V\sigma$ index represents the integer magnitude of TEC variability regarding quiet reference median in terms of σ grades. Here, the ionosphere quiet state is within $\Delta\text{TEC} < \pm 1\sigma$. If the value of instant TEC is outside of pre-defined bounds of $\mu \pm 1\sigma$, the anomaly of TEC is detected (Akhoondzadeh 2015).

The $V\sigma$ grade segmentation –4:1:4 is similar to the ionospheric weather W-index (Gulyaeva et al. 2013), yet it differs from W-index by the *dynamic* thresholds expressed through the variable standard deviation, σ. An advantage of $V\sigma$ index is that it is more physically justified showing ΔTEC in terms of the relevant standard deviation. This scenario can be easily implemented with any physical parameter, such as the ionospheric critical frequency, foF2, the peak electron density, NmF2, and the peak height, hmF2, using the relevant reference value (mean or median) and the standard deviation for the selected parameter.

Efficiency ($E\sigma$) of the ionosphere response to impact of earthquakes is represented by the relative density of the extreme negative indices $V\sigma n \leq -2$ ($mV\sigma n$) on the specified fragments of a map corresponding to decreased density of electrons $\Delta\text{TEC} \leq -1\sigma$ as compared with quiet reference state; or similarly, the extreme positive indices $V\sigma p \geq 2$ ($mV\sigma p$) on the selected fragments corresponding to increased density of electrons $\Delta\text{TEC} \geq +1\sigma$, to the total number of cells in the fragment(s) around the EQ hypocentre(s) on the map or series of EQs on the relevant maps (mtot):

$$E\sigma n = \frac{mV\sigma n}{mtot}, \quad E\sigma p = \frac{mV\sigma p}{mtot}. \tag{4}$$

In this study, the available GIM-TEC maps from 1999 to 2015 have been processed to produce output global maps of the 15-day sliding median μ, standard deviation σ, magnitudes $D\sigma$ and $V\sigma$ index in IONEX format with spatial resolution of $2.5° \times 5°$, in latitude and longitude, respectively. The histogram of annual frequency of occurrence of the specified magnitudes of $D\sigma$, in per cent, relative to the total number of about 45×10^6 grid elements per year (5183 grids $\times$ 24 h $\times$ DOY, with days-of-year, DOY, equal to 365 or 366) is plotted in Figure 1 in increments of 0.5σ. We note the asymmetry of the TEC enhancement ($D\sigma > 0$) and depletion ($D\sigma < 0$) occurrence. The sign of $D\sigma$ depicts ΔTEC for an instant TEC being either greater than or less than the quiet reference median. An appreciable number of 'quiet' TEC with $D\sigma = 0$ is also seen in Figure 1 when TEC is equal to the median value (Equation 3). There are negligible year-to-year (solar cycle) changes in $D\sigma$
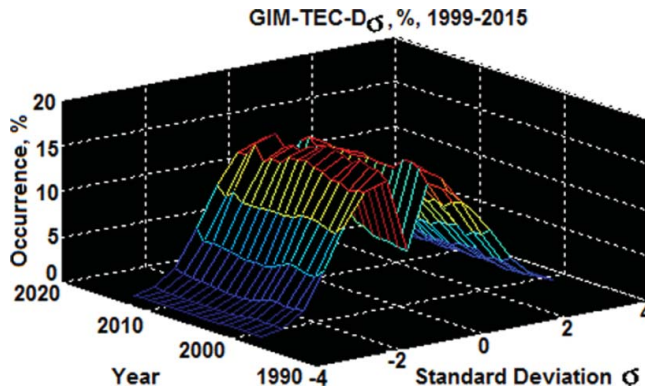
Figure 1. Histograms of annual percentage occurrence of deviation of TEC from the quiet reference-15-day sliding median normalized by the variability bounds σ in 0.5σ increments computed from GIM-TEC maps for the years from 1999 to 2015.

occurrence because of intrinsic σ variability in space and time involved in $D\sigma$ denominator normalizing ΔTEC at $D\sigma$ calculation. The moderate TEC variability is presented by $D\sigma$, which occurred between [-1σ:-2σ] and [$+1\sigma$:$+2\sigma$]. We note also a certain percentage of $D\sigma$ occurrences exceeding $\pm1\sigma$ which are denoted as TEC 'anomalies'.

The TEC data are extracted from GIM-TEC for the regions surrounding earthquake hypocentre at geographic latitude, θe, and geographic longitude, ϕe, within the radius of 1000 km, determined by $\theta \leq \theta e \pm 10°$, $\phi \leq \phi e \pm 7.5°$. The analysis of TEC for a rectangular region defined by (θ_i, ϕ_i) to (θ_s, ϕ_s) is provided by Gulyaeva et al. (2013, Appendix A) for the increments in θ and in ϕ given as $\Delta\theta$ and $\Delta\phi$, respectively. However, the space around the EQ hypocentre with radius of 1000 km is not a simple rectangular region. It is rather represented by fragments of 24 cells comprised of a square of 4 × 4 latitude/longitude grids and a rectangle of 8 × 2 latitude/longitude grids surrounding (θe, ϕe) as illustrated in Figure 2.
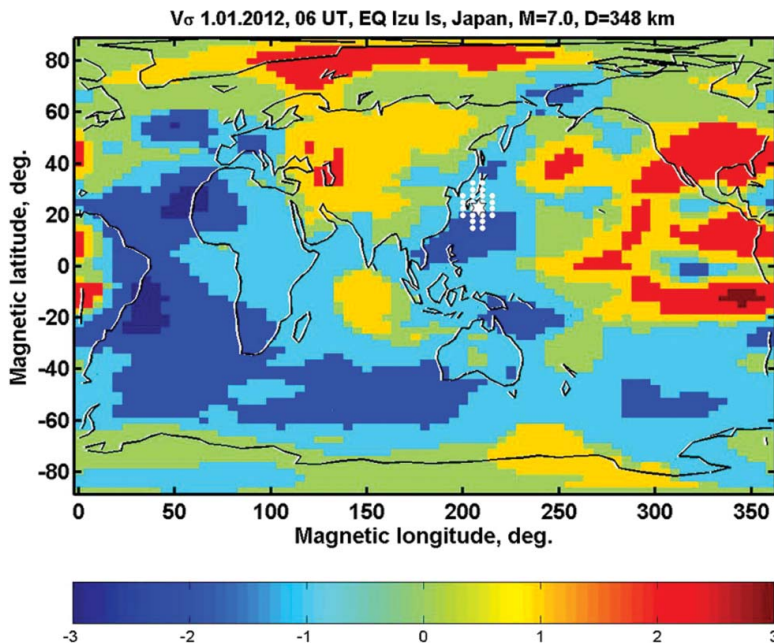

Figure 2. Global instantaneous $V\sigma$ map after deep Izu Islands, Japan, earthquake on 1 January 2012 at 06:00 UT. Earthquake hypocentre is indicated with a white star, and the region of analysis indicated with white points.

Global instantaneous $V\sigma$ map in geomagnetic coordinates frame for 1 January 2012, at 06:00 UT is presented in Figure 2 as an example of global variability index distribution. The time for the map, 06:00 UT, is an integer hour just after the Japan's Izu Islands earthquake on 1 January 2012, at 05:27:54 UT (14:40:27 LT) with $Mw = 7.0$, and at a depth of 348 km (Lin 2012). The hypocentre of the earthquake was at [31.4° N, 138.2° E] in geographic coordinates, and [22.8° N, 208.1° E] in geomagnetic coordinates which is close to the crest of the equatorial ionization anomaly (EIA). The area selected for the analysis is designated by white points on IONEX grids surrounding the earthquake hypocentre (white star) in Figure 2. This earthquake occurred under quiet geomagnetic conditions (see the next Section for the classification criteria) nevertheless there is appreciable negative $V\sigma$ anomaly southwards of the hypocentre which is detected earlier by Lin (2012) with the nonlinear principal component analysis (NLPCA) while the principal component analysis (PCA) was unable to detect the anomaly. The evaluation of the global distribution of earthquakes of $M6.0+$ under quiet conditions and the geomagnetic storms in the selected fragments of the globe surrounding the EQ hypocentre is provided in the next section.

3. Spatial distribution of earthquakes under quiet and storm conditions

The aim of the present study is to reveal a novel empirical evidence of the earthquake related TEC anomalies under quiet space weather conditions and geomagnetic storms. We use earthquake data from the global Catalogue of the Advanced National Seismic System (ANSS) provided by the Northern California Earthquake Data Center (NCEDC 2014). The composite Catalogue of earthquakes created by ANSS is a world-wide earthquake catalogue which is generated by merging the master earthquake catalogues from contributing ANSS member institutions and then, removing duplicate events, or non-unique solutions for the same event. We use the monthly and annual data for earthquakes of magnitude $M6.0$ to $M10.0$ from the NCEDS Catalogue for a period from January 1999, to December 2015, according to the availability of the hourly GIM-TEC maps during the solar cycles 23 and 24.

Comparison of earthquakes with the equatorial ring current disturbances has shown that the earthquakes occurred during the Disturbance Storm Time (Dst) storms comprise 13% of the total number of more than 79,000 earthquakes $M5.0+$ for 1964–2013 (Gulyaeva 2014). While the severity of a geomagnetic storm is defined by the Dst index which serves as a standard measure of the energy transfer from the solar wind to the ring current within the magnetosphere (Sugiura 1963), there are also other geomagnetic indices specifying impact on the ionosphere under quiet or disturbed conditions (Deminov et al. 2013). In this study, the EQ series and relevant $V\sigma$ quantities on a map are referred to the 'storm' conditions (Gonzalez et al. 1994) if at least one of the following criteria is satisfied assuming the 'non-storm' conditions otherwise:

$$AE_{\max} \geq 500 \text{ nT}, \ aa_{\max} > 45 \text{ nT}, \ ap_{\max} > 30 \text{ nT}, \ ap(\tau) > 18 \text{ nT}, \ Dst_{\min} \leq -30 \text{ nT}. \quad (5)$$

The above conditions should be fulfilled both for the nearest UT hour (or 3 h UT interval) following the earthquake and the nearest pre-earthquake hour (or 3 h UT interval) to capture storm or sub-storm impact at the time of EQ event. Here $AE_{\max}$ is the auroral electrojet AE value for two near-EQ hours, $aa_{\max}$ is the mid-latitude aa index value for a given and preceding 3 h intervals; $ap_{\max}$ is the maximum ap value for a given and preceding 3-h intervals. The $ap(\tau)$ is the mean weighted value of ap index (Wrenn 1987):

$$ap(\tau) = (1 - \tau)(ap_0 + ap_{-1}\tau + ap_{-2}\tau^2 + \cdots),$$

with the characteristic time $T = 11$ h or $\tau = \exp(-3/T) \approx 0.76$; $ap_0, ap_{-1},\ldots$ are ap values at a given time of EQ and preceding 3 h intervals. The $Dst_{\min}$ is the minimum disturbance storm time value

for 2 h near EQ time. All the above indices are expressed in nanoTeslas (nT). The periods of storms and sub-storms are included by Equation (5) which may occur at all latitudes from the pole (*AE* index) through the mid-latitudes (*aa*, *ap* and *ap(τ)* indices) to equator (Dst index). The global effect is confirmed by the correlation found between the variation in two independent processes occurring at widely separated regions in space, namely, the ring current intensity and the behaviour of ionospheric densities at high latitudes (Yadav & Pallamraju 2015).

From the total number of 2670 earthquakes of *M*6.0+ during 1999–2015, we have found the majority of events happened under quiet geomagnetic conditions (2205 'non-storm' earthquakes) and 465 'storm' earthquakes (17.4% of the total events list). We note that the per cent of *M*6.0+ storm-time earthquakes for a period of observation during 17 recent years exceeds the storm-time percentage (13%) of *M*5.0+ earthquakes for 50 years of observation (Gulyaeva 2014) due to the extended criteria for the 'storm' classification (Equation 5) than the former specification of the geomagnetic state according only to the ring current Dst storm occurrence.

The global spatial distribution of earthquakes is irregular tending to denser earthquake occurrence in the Pacific region (Levin & Sasorova 2012; Gulyaeva 2014). In the present study, we have estimated the spatial percentage distribution of the 'non-storm' earthquakes *M*6.0+ under quiet magnetosphere (Figure 3(a)) and the 'storm' earthquakes (Figure 3(b)) for 1999–2015. The 'non-storm' earthquakes distribution (Figure 3(a)) remind that of *M*5.0+ earthquake zones of enhanced seismic activity (Gulyaeva 2014) which are observed along the tectonic plates boundaries at longitudes from 90° to 190° E and magnetic latitudes from 40° S to 40° N, with dominant earthquake occurrence in the sub-equatorial region of the South magnetic hemisphere. The next appreciable zone of enhanced tectonic activity is revealed around the West coast of South America which also corresponds to a tectonic plate boundary. We note that most of the earthquakes are located within the limits of the closed magnetic field lines, which corresponds to $L = 4.17$ at the magnetic equator for GPS orbit (Lee et al. 2013) so the TEC variability within the low latitude and middle latitude regions represents the area for the co-seismic and post-seismic ionospheric and plasmaspheric effects.

The pattern of 'storm' earthquakes (Figure 3(b)) differs from the 'non-storm' map (Figure 3(a)) indicating extreme density of earthquake occurrence off the Pacific Coast of Japan (10% of total 'storm' events for 1999–2015). This is due to Tohoku *Mw*9.1 mega-earthquake occurred on 11 March 2011, 05:46:24 UT which is accompanied by successive 49 earthquakes (aftershocks) of *M*6.0+ during 11–15 March (Figure 4a, dashed area) listed in the NCEDS Catalogue (Komjathy et al. 2013; Xu et al. 2013; Devi et al. 2014; Nagao et al. 2014; NCEDC 2014). These 'storm' earthquakes occurred during a moderate Dst storm, which started on 10 March, 08:00 UT, and reached
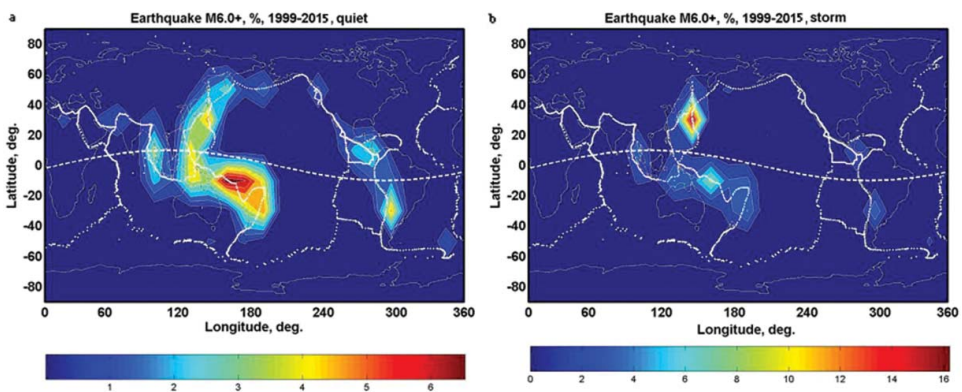

Figure 3. The zones of enhanced seismic activity for earthquakes *M*6.0+, in per cent, relative the earthquakes number for 1999–2015. (a) Earthquakes under quiet space weather conditions. (b) Earthquakes during the geomagnetic storms. Tectonic plate boundaries are indicated by bold points and the magnetic equator is denoted by the dashed line.
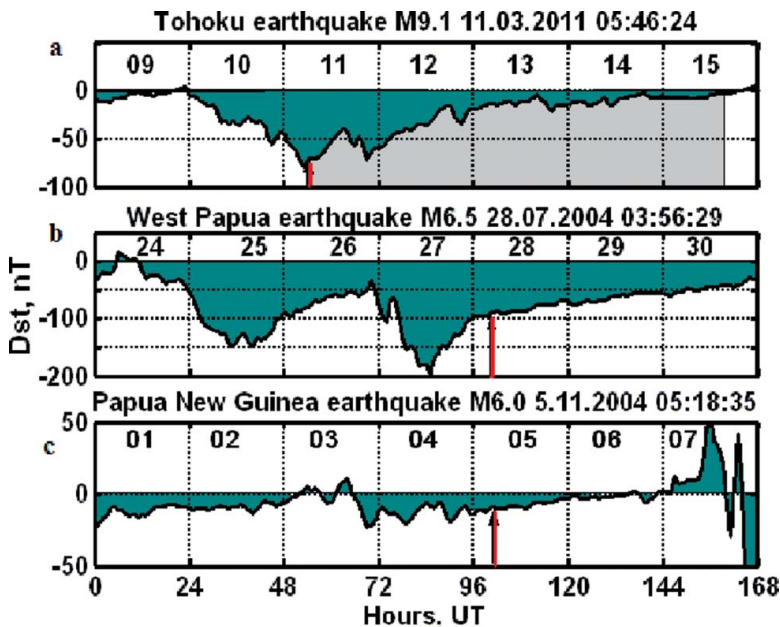
Figure 4. Graphs of the Dst index for three specific earthquakes: (a) Tohoku mega-earthquake *M*9.1 and the aftershocks of *M*6.0+ (shaded area) during moderate Dst storm; (b) West Papua earthquake *M*6.5 at a recovery of the severe Dst storm; and (c) Papua New Guinea earthquake M6.0 under quiet geomagnetic conditions.

its peak with Dst values as low as −80 nT on 11 March, 05:00 UT just before the Tohoku *M*9.1 earth-quake (arrow in Figure 4(*a*)) and the aftershocks repeated until the end of the recovery phase of the storm. The impact of magnetic storm on the aftershocks of the Tohoku mega-earthquake off the Pacific coast of Japan (Figures 3(*b*) and 4(*a*)) deserves special investigation (Devi et al. 2014).

Figure 4(*b,c*) illustrates two types of EQs under intense storm and quiet geomagnetic conditions, respectively, characterized by Dst index plots. Figure 4*b* refers to the 'storm' kind of EQ (*M*6.5, at a depth of 13.4 km) occurred on 28 July 2004, 03:56:29 UT, (12:48 LT) at West Papua, [0.44° S, 133.1° E] in geographic coordinates, and [9.0° S, 204.4° E] in geomagnetic coordinates. The Dst = −91 nT is shown by arrow in Figure 4(*b*) at the earthquake instant during the storm recovery follow-ing the storm peak of Dst = −197 nT on 27 July 2004, at 13:00 UT. An example of the 'non-storm' EQ (*M*6.0, at a depth of 125.7 km) is shown in Figure 4(*c*). The EQ occurred on 5 November 2004, 05:18:35 UT (14:54 LT) at Papua New Guinea, [4.36° S, 143.9° E] in geographic coordinates, and [12.8° S, 215.3° E] in geomagnetic coordinates, with Dst = −9 nT (Figure 4(*c*), arrow). Both exam-ples are observed under moderate solar activity with 12-monthly smoothed sunspot number R_{12} = 40.2 and 35.3, in July and November 2004, respectively. To keep the post-seismic TEC analysis under the typical 'storm' and 'non-storm' conditions, we have chosen the area surrounding each EQ within the radius of 1000 km around the hypocentre at the $V\sigma$ maps during 12 h after each EQ *M*6.0+ for the period of study, results of which are presented in the next section.

4. Results

Temporal–latitudinal graphs of TEC (upper panels) and $V\sigma$ (lower panels) during three days at the meridian of 85° E are intended to illustrate difference between 'storm' type and 'non-storm' states of the ionosphere parameters under consideration (Figure 5). Figure 5(*a,c*) (17–19 March 2015) refers to the VarSITI campaign for 'St. Patrick's Day 2015 Event' in which a strong geomagnetic super-storm occurred with AE_{max} > 2000 nT on 17 March 2015 at 14:00 UT. The Dst value got as low as − 228 nT on 18.03.2015 at 00:00 UT. There have been two 'storm' type EQs *M*6.2 (not shown here):
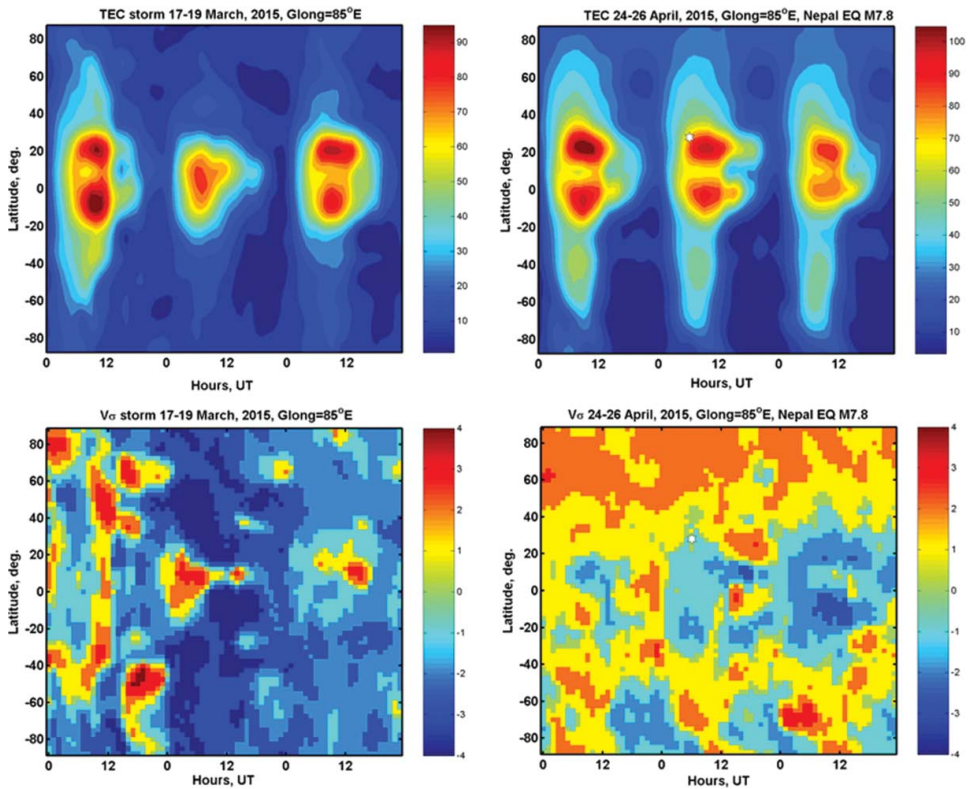
Figure 5. Temporal–latitudinal graphs of TEC (upper panels) and $V\sigma$ (lower panels) during three days at the meridian of 85° E: (a and c) the day before, during and after the peak of the intense ionosphere super-storm on 18 March 2015 at 07:00 UT; (b and d) the day before, during and after the Nepal earthquake on quiet day 25 April 2015 at 06:11 UT (white star at the EQ hypocentre).

the first earthquake occurred on 17 March 2015 at 22:12:29 UT at the geographic coordinates of [1.7° N, 126.5° E], and the second one occurred on 18 March 2015 at 18:27:30 UT, at [36.1° S, 73.5° W] in geographic coordinates. To demonstrate the ionosphere state at all panels at the same meridian, the subplots of Figure 5 are provided for geographic longitude of 85° E close to the Nepal EQ (Figure 5(b,c), 24–26 April 2015). The Nepal EQ $M7.8$ occurred on 25 April 2015 at 06:11:26 UT, at [28.1°N, 84.7°N] in geographic coordinates (star in graphs), and at [19.1° N, 158.9° E] in geomagnetic coordinates which is close to the crest of the Equatorial Ionosphere Anomaly (EIA) similar to the earthquake shown in Figure 2. Nepal EQ happened to be on the quietest day of the month, Q1, according to the International Geomagnetic Quiet/Disturbed Days Lists (http://wdc. kugi.kyoto-u.ac.jp/), so Figure 5(b,d) represents example of non-storm EQ.

An erosion and dissipation of TEC EIA is observed during the geomagnetic super-storm on 18 March (Figure 5(a)) which is normally represented by a two-humps-like latitudinal shape with two peaks at the crests of EIA at about ±15° in magnetic latitude with a minimum at magnetic equator which is observed in Figure 5(a) on 17 March and partially recovered on 19 March.

Though the Nepal EQ happened on the quiet day, the peak TEC at the South crest of EIA (the magnetic conjugate region for Nepal EQ hypocentre area) has been diminished, presumably, due to the EQ impact through the ionosphere conjugation. In particular, TEC at the South EIA peak is decreased from 102 TECU on 24 April to 62 TECU on 25 April and further decreased to 47 TECU on 26 April, i.e. day-to-day TEC depletion is observed after the EQ. More drastic differences between the 'storm' and 'non-storm' co-seismic ionosphere are observed with $V\sigma$ maps in Figure 5(c,d). In particular, most of the $V\sigma$ values on map are indicators of positive and negative TEC anomalies for

Table 2. Efficiency of ionosphere response, $E\sigma$, %, for the TEC enhancement and depletion, $V\sigma$, at the different ranges of EQ magnitude (M), at the nearest integer hour (UT) after EQ. The mean energy (J) and standard deviation std for the earthquakes number m are given for each collection during 1999–2015.

	Storm					Quiet				
M	m	$E\sigma n$	$E\sigma p$	Energy	std	m	$E\sigma n$	$E\sigma p$	Energy	std
$6.0 \leq M < 6.5$	327	20.9	25.0	1.22×10^{14}	6.0×10^{13}	1529	15.3	19.2	1.19×10^{14}	6.1×10^{13}
$6.5 \leq M < 7.0$	90	22.6	25.4	6.47×10^{14}	3.2×10^{14}	450	14.7	21.0	6.84×10^{14}	3.5×10^{14}
$7.0 \leq M < 7.5$	31	19.9	24.3	3.78×10^{15}	1.9×10^{15}	147	16.2	18.0	3.92×10^{15}	2.1×10^{15}
$7.5 \leq M < 8.0$	16	24.6	27.9	2.42×10^{16}	9.8×10^{15}	61	18.4	18.6	2.06×10^{16}	9.9×10^{15}
$8.0 \leq M < 10.0$	1	8.4	47.3	1.78×10^{17}	–	18	15.3	16.1	2.22×10^{17}	2.3×10^{17}
Total $M6.0+$	465	21.2	25.2	7.74×10^{15}	1.3×10^{17}	2205	15.3	19.4	3.77×10^{15}	5.1×10^{16}

the 'St. Patrick's Day 2015 Event' (Figure 5c) while $V\sigma$ is quiet on 25 April during 12 h after EQ which refers to the time slot used for the further analysis in the present study.

We proceed to statistical evaluation of the $V\sigma$ signatures under the 'storm' and 'non-storm' conditions in the region of interest. Table 2 presents efficiency $E\sigma$, in per cent (Equation 4) of EQ impact on TEC anomalies at the nearest integer UT hour after the EQ in several ranges of EQ magnitudes from $M6.0$ to $M10.0$ in step of $\Delta M = 0.5$ M units except for the greatest EQ magnitudes $M \geq 8.0$ to $M10.0$. Overall $E\sigma$ value for each subset is also provided in the last row of Table 2.

As can be seen in Table 2, the efficiency of EQ impact on TEC anomalies increases as EQ magnitude, M, gets larger for the both negative $V\sigma n$ occurrence and positive $V\sigma p$ occurrence around the EQ hypocentres. The total energy emitted by an earthquake (E, in Joules) (Gutenberg & Richter 1956) is in exponential relation with the magnitude (M) represented by the equation: $\log E = 1.5M + 4.8$ which is applied in the present study for calculation of EQ emitted energy for individual EQ events. The mean energy and the standard deviation are provided for each subset in Tables 2 and 4. The increasing efficiency of the EQ impact on TEC anomalies in terms of M (Table 2) is coherent with the amount of energy allocated during an earthquake (Bath 1956; Levin & Sasorova 2012; Swedan 2015) which gets larger with increasing M as presented in Table 2. This result supports numerous studies on seismic–ionospheric associations because it presents straightforward evidence on dependence of co-seismic TEC variability on amount of EQ energy. The EQ allocated energy is the primary reason for $E\sigma$ dependence on M in our results because all EQs of any magnitude ($M6.0+$) in either subset are analysed with the same algorithm using the derived $V\sigma$ index in the vicinity of hypocentre under specified level of geomagnetic activity. Also, it follows from Table 2 that the efficiency of positive TEC anomalies is greater than the negative ones which testifies on the dominant EQ-related plasma density enhancements as compared with its depletion. The storm-time efficiency is larger than the non-storm results which bring the evidence that the ionospheric–geomagnetic storms facilitate TEC enhancements or depletion induced by EQs.

We specify $V\sigma$ results for daytime earthquakes (the solar zenith angle $\chi < 90°$) and nighttime conditions (the solar zenith angle $\chi > 90°$) during 12 h after EQ for the both 'storm' and 'non-storm' classes. The time variation of efficiency $E\sigma$ (Equation (4)) after EQ is provided in Figure 6 for daytime, nighttime and total diurnal variation. Symbol S+ in the plots stands for the positive 'storm' $V\sigma p$, Q+ for quiet 'non-storm' $V\sigma p$, S- for the negative 'storm' $V\sigma n$, and Q- for the negative quiet $V\sigma n$. Points on the 'Total' subplot curves at 0 h are those values that are listed in the last row of Table 2.

In general, all statistical results for the quiet and storm conditions confirm existence of seismic - ionospheric associations since the efficiency of EQ impact on TEC anomalies is not zero in all cases. For some individual EQs, the TEC anomalies in the sense defined in the present study could be missed in the EQ predefined area within 1000 km radius from the hypocentre but we should keep in mind that the most notable ionosphere variability anomalies are specific for the high latitudes while the EQs regions of occurrence belong to the middle and low latitudes. The most important outcome of results in Figure 6 is that efficiency of EQs on positive
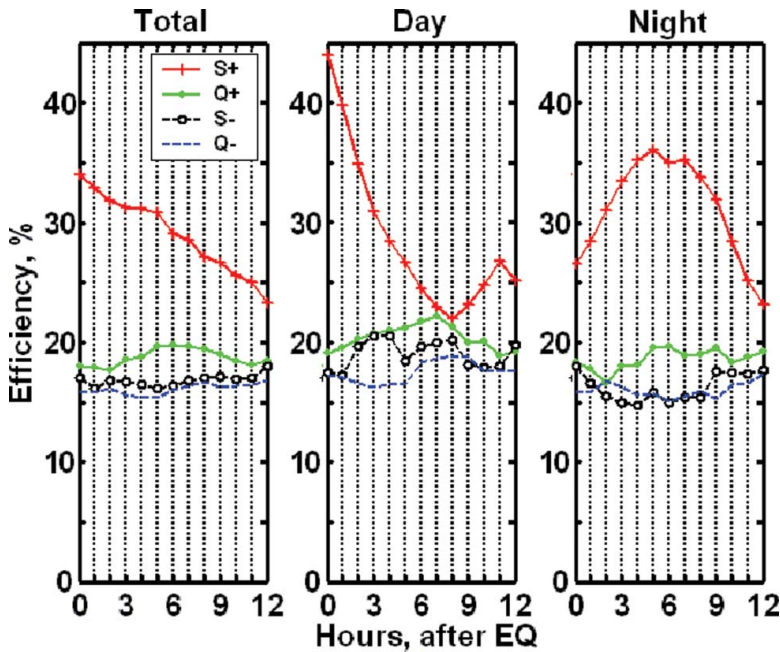
Figure 6. Efficiency of the seismic impact on the ionosphere for 12 h after earthquakes with $V\sigma$ index anomalies for nighttime, daytime and the total data-set under quiet conditions and during the geomagnetic storms.

TEC anomalies under storm condition is twice as large as those under non-storm anomalies. Peak of $E\sigma$ for storm $V\sigma p$ occurs by daytime (and total diurnal variation) at the nearest ($t = 0$) hour after EQ. The value decreases after the EQ to the level of other cases as indicated in Figure 6. When compared with the daytime, the results for nighttime storm $V\sigma p$ anomalies show an enlargement peak by 6 h after the EQ with a value which is twice as large as the other levels and it decreases during the 6 h after the peak.

The mean curves of efficiency of EQ impact on TEC anomalies (Figure 6) are accompanied by Table 3 depicting the ANOVA (Analysis of Variance) statistical results for Vp and Vn occurrence under quiet and disturbed geomagnetic conditions for post-earthquake hours within the 1000 km radius around the hypocentre. Here F implies Fisher's criteria, and p is the probability of the result assuming the null hypothesis. Analysis of variance (ANOVA) is a collection of statistical models used to analyse the differences among group means and their associated procedures (such as 'variation' among and between groups). In the ANOVA setting, the observed variance in a particular variable is partitioned into components attributable to different sources of variation. In its simplest form, ANOVA provides a statistical test of whether or not the means of several groups are equal, and therefore generalizes the t-test to more than two groups. ANOVA is applied here for comparing

Table 3 ANalysis Of VAriance (ANOVA) results for *Vp* and *Vn* occurrence under quiet and disturbed geomagnetic conditions at post-eathquake hours within the 1000 km radius around the hypocentre: F – Fisher's criteria, *p* – the probability of the result assuming the null hypothesis.

| | Quiet conditions | | | | Geomagnetic storms | | | |
| | *Vp* | | *Vn* | | *Vp* | | *Vn* | |
	F	*p*	*F*	*p*	*F*	*p*	*F*	*p*
Day	0.6365	0.59	0.3135	0.82	0.4480	0.72	0.6551	0.58
Night	0.1470	0.93	0.1375	0.94	0.7892	0.50	0.2528	0.86
Total	0.2236	0.88	0.0754	0.97	0.8248	0.48	0.4642	0.71

Table 4. Mean energy E (J) and standard deviation, std, of earthquakes for five ranges of EQ magnitude (M) three ranges of hypo-centre depth (D in km), observed under geomagnetic quiet conditions and geomagnetic storms during 1999–2015. Three classes of epicentre depth, D, are grouped as: $D1 \leq 70$ km; $70 < D2 \leq 300$ km; $300 < D3 \leq 800$ km, m indicates the number of EQ events.

M	m	E	std	m	E	std	m	E	std	Σm
		Quiet conditions								2205
Daytime		$D1$			$D2$			$D3$		1121
6.0:6.5	607	1.19×10^{14}	6.0×10^{13}	106	1.22×10^{14}	6.3×10^{13}	57	1.23×10^{14}	6.1×10^{13}	770
6.5:7.0	191	6.71×10^{14}	3.2×10^{14}	21	7.52×10^{14}	3.2×10^{14}	25	7.39×10^{14}	4.0×10^{14}	237
7.0:7.5	51	3.91×10^{15}	2.2×10^{15}	15	3.83×10^{15}	1.9×10^{15}	7	4.07×10^{15}	1.4×10^{15}	73
7.5:8.0	22	2.19×10^{16}	1.0×10^{16}	5	2.20×10^{16}	1.2×10^{16}	5	1.75×10^{16}	4.3×10^{15}	32
8.0:9.0	8	1.59×10^{17}	1.4×10^{17}	–	–	–	1	1.78×10^{17}	–	9
Nighttime		$D1$			$D2$			$D3$		1084
6.0:6.5	626	1.18×10^{14}	6.2×10^{13}	96	1.22×10^{14}	5.9×10^{13}	37	1.07×10^{14}	6.2×10^{13}	759
6.5:7.0	166	6.86×10^{14}	3.6×10^{14}	29	6.98×10^{14}	3.9×10^{14}	18	6.32×10^{14}	3.0×10^{14}	213
7.0:7.5	56	3.84×10^{15}	2.1×10^{15}	10	4.59×10^{15}	2.2×10^{15}	8	3.66×10^{15}	1.6×10^{15}	74
7.5:8.0	22	2.11×10^{16}	1.0×10^{16}	5	1.62×10^{16}	7.9×10^{15}	2	1.58×10^{16}	–	29
8.0:9.0	9	2.83×10^{17}	2.9×10^{17}	–	–	–	–	–	–	9
					Geomagnetic storms					465
Daytime		$D1$			$D2$			$D3$		229
6.0:6.5	138	1.23×10^{14}	6.1×10^{13}	9	1.16×10^{14}	4.3×10^{13}	9	1.29×10^{14}	6.6×10^{13}	156
6.5:7.0	38	6.62×10^{14}	3.4×10^{14}	4	6.92×10^{14}	4.2×10^{14}	5	9.36×10^{14}	4.4×10^{14}	47
7.0:7.5	16	3.60×10^{15}	1.7×10^{15}	1	5.62×10^{15}	–	1	7.94×10^{15}	–	18
7.5:8.0	8	2.41×10^{16}	1.2×10^{16}	–	–	–	–	–	–	8
8.0:9.0	–	–	–	–	–	–	–	–	–	–
Nighttime		$D1$			$D2$			$D3$		236
6.0:6.5	134	1.20×10^{14}	6.0×10^{13}	24	1.27×10^{14}	6.3×10^{13}	13	1.17×10^{14}	5.8×10^{13}	171
6.5:7.0	34	6.27×10^{14}	2.7×10^{14}	7	4.77×10^{14}	1.5×10^{14}	2	5.01×10^{14}	–	43
7.0:7.5	11	3.15×10^{15}	1.7×10^{15}	–	–	–	2	5.62×10^{15}	–	13
7.5:8.0	5	2.35×10^{16}	7.1×10^{15}	1	–	–	2	2.24×10^{16}	–	8
8.0:9.0	1	1.78×10^{17}	–	–	–	–	–	–	–	1

(testing) Vp and Vn groups for statistical significance. The p-values in Table 4 show that the selected algorithm of Vp and Vn estimates is meaningful according to the variables.

To determine the dependence of ionosphere variability on the depth of the EQ hypocentre, the relations of the different magnitudes of EQs with their depth are evaluated. The EQs occurrence for the different ranges of the hypocentre depth in the Pacific region is provided in detail by Levin and Sasorova (2012). The results of evaluation of the earthquake energy and standard deviation for three categories of depths for daytime and nighttime under geomagnetic quiet and storm conditions for 1999–2015 are given in Table 4. Hypocentre depth, D, is grouped into three classes: the shallow depth, $D1 \leq 70$ km; the descent depth, $70 < D2 \leq 300$ km; the deep depth, $300 < D3 \leq 800$ km. The occurrence of EQs decreases with increasing depth both for geomagnetic quiet conditions and storms. While the magnitude M is introduced by Gutenberg and Richter (1956) as a measure of energy emitted by EQ, the specification of energy distribution in terms of the depth categories shows the dependence of EQs energy on depth so that the energy of EQs gets larger as the depth increases.

5. Conclusion

In this study, the structural changes of ionosphere are investigated with respect to disturbances in the ionization levels and geomagnetic field due to storms and earthquakes using a novel $V\sigma$ index, which is derived using the variability of GIM-TEC. The seismic-ionospheric associations are analysed during 12 h after each of 2670 earthquakes of Richter magnitude from $M6.0$ to $M10.0$ separated to 'storm' class of 465 EQs and 'quiet' or 'non-storm' class of 2205 EQs worldwide from January 1999 to December 2015.

The median, μ, of 15 days prior to the current day at each cell of GIM-TEC map in $2.5° \times 5°$ of latitude / longitude grids is computed for each hour UT (0, 1, ..., 23 h) as a reference value. The standard deviation σ from the median represents a measure of the dispersion of distribution. The deviation of instant TEC from the median normalized by the standard deviation, $D\sigma$, is converted into an index, $V\sigma$, varying from -4 to $+4$, that corresponds to extreme negative or positive deviations, respectively.

Efficiency ($E\sigma$) of the ionosphere response to impact of earthquakes is estimated as a relative density of the negative indices $V\sigma n \leq -2$ on the specified fragments of a map ($\Delta TEC \leq -1\sigma$), or the positive indices $V\sigma p \geq 2$ ($\Delta TEC \geq +1\sigma$), regarding the total number of cells in the fragment(s) of 1000 km radius around the EQ hypocentre(s) on the map or series of EQs on the relevant maps.

It is found that the efficiency of EQ impact on the ionosphere is growing with EQ magnitude M at the nearest integer hour UT after EQ both for the storm and non-storm classes. The positive TEC anomalies are more effective than the negative ones for both storm and non-storm subsets which indicate on the EQ post-effects producing rather increased plasma variability in the ionosphere than its decreasing process.

The $V\sigma$ values grouped with respect to storm-time earthquakes and quiet-time earthquakes for nighttime (solar zenith angle $\chi > 90°$) and daytime ($\chi < 90°$) occurrences during 12 h after EQ show that post-seismic TEC positive anomalies occur almost twice as much as compared to the negative anomalies under storm conditions. Twice as many positive TEC anomalies during geomagnetic storm in the near-hypocentre region are observed at the first integer hour in UT after EQ with a subsequent decrease during 12 h afterwards for daytime. The increase of TEC positive anomalies by nighttime is observed during 6 h after EQ followed by a gradual recovery after the peak.

Analysis of the EQs energy for three classes of the depth ($D \leq 70$ km, 70:300 km, 300:800 km) brought an evidence of its dependence on the depth of the tectonic events. While the magnitude M is introduced by Gutenberg and Richter (1956) as a measure of energy E emitted by EQ, $M \sim M(E)$, the specification of energy distribution in terms of the depth categories shows the energy of EQs growing with the greater depth D, in other words, the EQ magnitude should be represented in a function of two variables: $M \sim M(E,D)$.

The present results suggest that there is a challenge for more sophisticated techniques to be developed in order to distinguish the earthquake effects on the ionosphere happened on the background of geomagnetic activity. The results of this study will be used as a basis for observing and grouping the disturbances in the ionosphere and geomagnetic field and $V\sigma$ index can be developed further as a storm and/or earthquake precursor.

Disclosure statement

No potential conflict of interest was reported by the authors.

ORCID

Tamara Gulyaeva http://orcid.org/0000-0002-4756-6066
Feza Arikan http://orcid.org/0000-0002-6481-1385

References

Afraimovich E, Astafyeva E. 2008. TEC anomalies – local TEC changes prior to earthquakes or TEC response to solar and geomagnetic activity changes? Earth Planets Space. 60:961–966.

Akhoondzadeh M. 2015. Firefly Algorithm in detection of TEC seismo-ionospheric anomalies. Adv Space Res. 56:10–18, DOI:10.1016/j.asr.2015.03.025.

Arikan F, Deviren MN, Lenk O, Sezen U, Arikan O. 2012. Observed Ionospheric Effects of 23 October 2011 Van Turkey Earthquake. Geomatics, Natural Hazards, Risk. 3:1–8.

Artu J, Lognonné P, Blanc E. 2001. Normal modes modeling of post-seismic ionospheric oscillations. Geophys Res Lett. 28:697–700. DOI: 10.1029/2000GL000085.

Astafyeva E, Heki K. 2009. Dependence of waveform of near-field coseismic ionospheric disturbances on focal mechanisms. Earth Planet Space. 61:939–943.

Astafyeva E, Heki K, Afraimovich E, Kiryushkin V, Shalimov S. 2009. Two-mode long-distance propagation of coseismic ionosphere disturbances. J Geophys Res. 114:A10307. DOI: 10.1029/2008JA013853.

Astafyeva E, Shalimov S, Olshanskaya E, Lognonné1 P. 2013. Ionospheric response to earthquakes of different magnitudes: Larger quakes perturb the ionosphere stronger and longer. Geophys Res Lett. 40:1675–1681, DOI: 10.1002/grl.50398.

Athanasiou MA, Anagnostopoulos GC, Iliopoulos AC, Pavlos GP, David CN. 2011. Enhanced ULF radiation observed by DEMETER two months around the strong 2010 Haiti earthquake. Nat Hazards Earth Syst Sci. 11:1091–1098. DOI: 10.5194/nhess-11-1091-2011.

Bath M. 1956. Evaluation of seismicity. Bul Seismol Soc America. 46:217.

Chen YI, Liu JY, Tsai YB, Chen CS. 2004. Statistical tests for pre-earthquake ionospheric σ. Terr Atmos Oceanic Sci. 15:385–396.

Davies K, Baker DM. 1965. Ionospheric effects observed around the time of the Alaskan earthquake of March 28, 1964. J Geophys Res. 70:2251–2263.

Deminov MG, Deminova GF, Zherebtsov GA, Polekh NM. 2013. Statistical properties of variability of the quiet ionosphere F2-layer maximum parameters over Irkutsk under low solar activity. Adv Space Res. 51:702–711. DOI: 10.1016/j.asr.2012.09.037.

Depueva AKh, Mikhailov AV, Devi M, Barbara AK. 2007. Spatial and time variation in critical frequencies of the ionospheric F region above the zone of equatorial earthquake preparation. Geomagn Aeronomy. 47:129–133. DOI: 10.1134/S0016793207010197.

Devi M, Barbara AK, Oyama K-I, Chen Ch-H. 2014. Earthquake induced dynamics at the ionosphere in presence of magnetic storm. Adv Space Res. 53:609–618. DOI: 10.1016/j.asr.2013.11.054.

Freund F. 2013. Earthquake forewarning – a multidisciplinary challenge from the ground up to space. Acta Geophys. 61:775–807. DOI: 10.2478/s11600-013-0130-4.

Gonzalez WD, Joselyn JA, Kamide Y, Kroehl HW, Rostoker G, Tsurutani BT, Vasyliunas VM. 1994. What is geomagnetic storm? J Geophys Res. 99:5771–5792.

Gulyaeva TL. 2014. Association of seismic activity with solar cycle and geomagnetic activity. Develop Earth Sci. 2:14–19. Available from: http://www.seipub.org/des/.

Gulyaeva TL, Arikan F, Hernandez-Pajares M, Stanislawska I. 2013. GIM-TEC adaptive ionospheric weather assessment and forecast system. J Atmos Solar-Terr Phys. 102:329–340. DOI: 10.1016/j.jastp.2013.06.011.

Gulyaeva TL, Arikan F, Hernandez-Pajares M, Veselovsky IS. 2014. North-South components of the annual asymmetry in the ionosphere. Radio Sci. 49:485–496. DOI: 10.1002/2014RS005401.

Gutenberg B, Richter CF. 1956. Magnitude and energy of earthquakes. Ann Geofis. 9:1–15.

Harrison RG, Aplin KL, Rycroft MJ. 2010. Atmospheric electricity coupling between earthquake regions and the ionosphere. J Atmos Sol-Terr Phys. 72:376–381. DOI: 10.1016/j.jastp.2009.12.004.

Hayakawa M, Hobara Y. 2010. Current status of seismo-electromagnetics for short-term earthquake prediction. Geomatics, NaturHazards Risk, 1:115–155. DOI:10.1080/19475705.2010.486933.

Hegai VV, Kim VP, Liu JY. 2006. The ionospheric effect of atmospheric gravity waves excited prior to strong earthquake. Adv Space Res. 37:653–659. DOI: 10.1016/j.asr.2004.12.049.

Heki K, Enomoto Y. 2015. Mw dependence of the preseismic ionospheric electron enhancements. J Geophys Res Space Phys. 120:7006–7020,. DOI: 10.1002/2015JA021353.

Hernandez-Pajares M, Juan JM, Sanz J, Garcia-Rigo A, Feltens J, Komjathy A, Schaer SC, Krankowski A. 2009. The IGS VTEC maps: a reliable source of ionospheric information since 1998. J Geodesy. 83:263–275.

Johnston MJS, Mueller RJ, Keller V. 1981. Preseismic and coseismic magnetic field measurements near the Coyote Lake, California, earthquake of August 6, 1979. J Geophys Res B2. 86:921–926. DOI: 10.1029/JB086iB02p00921.

Karatay S, Arikan F, Arikan O. 2010. Investigation of total electron content variability due to seismic and geomagnetic disturbances in the ionosphere. Radio Sci. 45:RS5012. DOI: 10.1029/2009RS004313.

Koshevaya SV, Perez-Enriquez R, Kotsarenko NYa. 1997. The detection of electromagnetic processes in the ionosphere caused by seismic activity. Geofisica Int., 36:55–60.

Komjathy A, Galvan DA, Stephens P, Butala MD, Akopian V, Wilson B, Verkhoglyadova O, Mannucci AJ, Hickey M. 2013. Detecting ionospheric TEC perturbations caused by natural hazards using a global network of GPS receivers: The Tohoku case study. Earth Planets Space. 64:1287–1294. DOI: 10.5047/eps.2012.08.003.

Koshevaya S, Grimalsky V, Urquiza1 G, Tecpoyotl M, Kotsarenko A, Yutsis V, Makarets N. 2012. Explosions and seismic phenomena based on exciting of acoustic-electromagnetic waves. Natural Sci. 4:652–658.

Kuo C, Huba J, Joyce G, Lee L. 2011. Ionosphere plasma bubbles and density variations induced by pre-earthquake rock currents and associated surface charges. J Geophys Res. 116:A10317. DOI: 10.1029/2011JA016628.

Le H, Liu JY, Liu L. 2011. A statistical analysis of ionospheric anomalies before 736 M6.0 earthquakes during 2002–2010. J Geophys Res. 116:A02303. DOI: 10.1029/2010JA015781.

Lee H-B, Jee G, Kim YH, Shim JS. 2013. Characteristics of global plasmaspheric TEC in comparison with the ionosphere simultaneously observed by Jason-1 satellite, J Geophys Res Space Phys. 118:935–946. DOI:10.1002/jgra.50130.

Levin BW, Sasorova EV. 2012. Seismichnost Tikhookeanskogo regiona: vijavleniye globalnikh zakonomernostey [Seismicity of the Pacific Region: global feature detection]. Moscow: Janus-K, pp. 307

Lin J-W. 2010. Two-dimensional ionospheric total electron content map (TEC) seismo-ionospheric anomalies through image processing using principal component analysis, Adv. Space Res. 45:1301–1310. DOI:10.1016/j.asr.2010.01.029.

Lin J-W. 2012. Nonlinear principal component analysis in the detection of ionospheric electron content anomalies related to a deep earthquake (>300 km, M 7.0) on 1 January 2012, Izu Islands, Japan, J Geophys Res Space Phys. 117:A06314. DOI:10.1029/2012JA017614.

Liu JY, Chen YI, Chuo YJ, Chen CS. 2006a. A statistical investigation of preearthquake ionospheric anomaly. J Geophys Res Space Phys. 111:A05304. DOI: 10.1029/2005JA011333.

Liu JY, Chen CH, Chen YI, Yen HY, Hatton K, Yumoto K. 2006b. Seismo-geomagnetic anomalies and $M \geqslant 5.0$ earthquakes observed in Taiwan during 1988–2001. Phys Chem Earth Part A/B/C. 31:215–222. DOI: 10.1016/j.pce.2006.02.009.

Liu J, Huang J, Zhang X. 2014. Ionospheric perturbations in plasma parameters before global strong earthquakes. Adv Space Res. 53:776–787. DOI: 10.1016/j.asr.2013.12.029.

Mannucci AJ, Wilson BD, Yuan DN, Ho CM, Lindqwister UJ, Runge TF. 1998. A global mapping technique for GPS-derived ionospheric TEC measurements. Radio Sci. 33:565–582.

Marekova E. 2014. Analysis of the spatial distribution between successive earthquakes occurred in various regions in the world. Acta Geophys. 62:1262–1282. DOI: 10.2478/s11600-014-0234-5.

Mukhtarov P, Andonov B, Pancheva D. 2013. Global empirical model of TEC response to geomagnetic activity. J Geophys Res Space Phys. 118:6666–6685. DOI:10.1002/jgra.50576.

Nagao T, Orihara Y, Kamogawa M. 2014. Precursory Phenomena Possibly Related to the 2011 M9.0 off the Pacific Coast of Tohoku Earthquake. J Disaster Res., 9:303–310.

Namgaladze AA, Zolotov OV, Karpov MI, Romanovskaya YV. 2012. Manifestations of the earthquake preparations in the ionosphere total electron content variations. Doklady Acad Sci Nat Sci. 4:848–855. DOI: 10.4236/ns.2012.411113.

NCEDC (2014), Northern California Earthquake Data Center. UC Berkeley Seismological Laboratory. Dataset. doi: 10.7932/NCEDC

Perevalova NP, Sankov VA, Astafyeva EI, Zhupityaeva AS. 2014. Threshold magnitude for Ionospheric TEC response to earthquakes. J Atmos Solar-Terr Phys. 108:77–90.

Pohunkov AA, Tulinov GF, Pohunkov SA, Rybin VV. 2013. Issledovanie vlijaniya sejsmicheskoy activnosti na ionniy sostav verkhney ionosferi [Investigation of seismic activity impact on the chemical composition of the upper ionosphere]. Heliogeophysical Res. 3:90–98. (in Russian).

Pulinets SA, Legen'ka AD, Gaivoronskaya TV, Depuev VKh. 2003. Main phenomenological features of ionospheric precursors of strong earthquakes. J Atmos Sol Terr Phys. 65:1337–1347.

Pulinets S, Boyarchuk K. 2004. Ionospheric precursors of earthquakes. Berlin: Springer-Verlag.

Pulinets S, Davidenko D. 2014. Ionospheric precursors of earthquakes and global electric circuit. Adv Space Res. 53:709–723. DOI: 10.1016/j.asr.2013.12.035.

Ralchovski TM, Christolov LV. 1985. On low-frequency radio emission during earthquakes. CR Acad Bulg Sci. 38:863–865.

Rishbeth H. 2006. Ionoquakes: Earthquake Precursors in the Ionosphere? EOS. 87:316–317.

Sugiura M. 1963. Hourly values of equatorial Dst for the IGY, NASA Rept. X-611-63-131. MD: NASA Goddard Space Flight Center.

Swedan NH. 2015. Ridge push engine of plate tectonics. Geotectonics. 49:342–359. DOI: 10.1134/S0016852115040081

Uyeda S, Nagao T, Kamogawa M. 2009. Short-term earthquake prediction: Current status of seismo-electromagnetics. Tectonophysics. 470:205–213. DOI: 10.1016/j.tecto.2008.07.019.

Varotsos P, Alexopoulos K. 1984a. Physical properties of the variations of the electric field of the earth preceding earthquakes, I. Tectonophysics. 110:73–98. DOI:10.1016/0040-1951(84)90059-3.

Varotsos P, Alexopoulos K. 1984b. Physical properties of the variations of the electric field of the earth preceding earthquakes, II. determination of hypocenter and magnitude. Tectonophysics. 110:99–125. DOI: 0040-1951(84)90060-X.

Varotsos PA, Sarlis NV, Skordas ES, Lazaridou MS. 2008. Fluctuations, under time reversal, of the natural time and the entropy distinguish similar looking electric signals of different dynamics. J Appl Phys. 103:014906. DOI:10.1063/1.2827363.

Varotsos PA, Sarlis NV, Skordas ES. 2009. Detrended fluctuation analysis of the magnetic and electric field variations that precede rupture. Chaos 19:023114. DOI:10.1063/1.3130931.

Varotsos P., Sarlis NV, Skordas ES, Uyeda S, Kamogawa M. 2011. Natural time analysis of critical phenomena. Proc Natl Acad Sci USA, 108(28):11361–11364. DOI:10.1073/pnas.1108138108.

Wrenn GL. 1987. Time-weighted accumulations ap(τ) and kp(τ). J Geophys Res. 92:10125–10129.

Xu G, Han P, Huang Q, Hattori K, Febriani F, Yamaguchi H. 2013. Anomalous behaviors of geomagnetic diurnal variations prior to the 2011 off the Pacific coast of Tohoku earthquake (Mw9.0). J Asian Earth Science. 77:59–65. DOI: 10.1016/j.jseaes.2013.08.011.

Yadav S, Pallamraju D. 2015. On the coupled interactions between ring current intensity and high-latitude ionospheric electron density variations. J Atmos Solar-Terr Phys. 125:50–58. DOI: 10.1016/j.jastp.2015.02.006.

Yen H-Y, Chen C-H, Yeh Y-H, Liu J-Y, Lin C-R, Tsai YB. 2004. Geomagnetic fluctuations during the 1999 Chi-Chi earthquake in Taiwan. Earth Planets Space. 56:39–45.